OXFORD

Cerebral Cortex, 2024, **34**, bhae083
https://doi.org/10.1093/cercor/bhae083
Advance access publication date 15 March 2024
Original Article

Hippocampal ripples coincide with "up-state" and spindles in retrosplenial cortex

Rafael Pedrosa[1,*], Mojtaba Nazari[2], Loig Kergoat[3,4], Christophe Bernard[3], Majid Mohajerani[2], Federico Stella[1], Francesco Battaglia[1,*]

[1]Donders Institute for Brain Cognition and Behaviour, Radboud University, Nijmegen 6525AJ, The Netherlands
[2]Canadian Centre for Behavioral Neuroscience, University of Lethbridge, Lethbridge AB T1K 6 3M4, Canada
[3]INSERM, INS, Institut de Neurosciences des Systèmes, Aix Marseille Université, UMR_S 1106, Marseille 13005, France
[4]Panaxium SAS, Aix-en-Provence 13100, France
*Corresponding authors: Donders Institute for Brain, Cognition and Behaviour, Neuroinformatica, Radboud University, Heyendaalseweg 135, Internal postal code: 66, 6525 AJ Nijmegen, The Netherlands. Email: rhapedrosa@gmail.com (Rafael Pedrosa); Email: F.Battaglia@science.ru.nl (Francesco Battaglia)

During NREM sleep, hippocampal sharp-wave ripple (SWR) events are thought to stabilize memory traces for long-term storage in downstream neocortical structures. Within the neocortex, a set of distributed networks organized around retrosplenial cortex (RS-network) interact preferentially with the hippocampus purportedly to consolidate those traces. Transient bouts of slow oscillations and sleep spindles in this RS-network are often observed around SWRs, suggesting that these two activities are related and that their interplay possibly contributes to memory consolidation. To investigate how SWRs interact with the RS-network and spindles, we combined cortical wide-field voltage imaging, Electrocorticography, and hippocampal LFP recordings in anesthetized and sleeping mice. Here, we show that, during SWR, "up-states" and spindles reliably co-occur in a cortical subnetwork centered around the retrosplenial cortex. Furthermore, retrosplenial transient activations and spindles predict slow gamma oscillations in CA1 during SWRs. Together, our results suggest that retrosplenial–hippocampal interaction may be a critical pathway of information exchange between the cortex and hippocampus.

Key words: default mode network; cortical spindle; hippocampus; retrosplenial cortex; sharp-wave ripple.

Introduction

The consolidation of newly encoded memories, facilitating their long-term retention, is thought to take place mostly during sleep (Stickgold and Walker 2005; Born and Wilhelm 2012) and, more specifically, to be based on the bidirectional interaction between the hippocampus and neocortex. Such interaction is thought to occur predominantly during non-rapid eye movement sleep (NREM) (Rolls 2000; Wang and Morris 2010; Girardeau et al. 2014). The replay of neural ensembles in the hippocampus (Wilson and McNaughton 1993; Nádasdy et al. 1999; Foster and Wilson 2006; Ólafsdóttir et al. 2016) as well as the repeated activation of cortical patterns (Peigneux et al. 2004; Tambini and Davachi 2019; Higgins et al. 2021) support this view. However, the physiological and dynamical properties of this interaction remain largely unknown. Several arguments point to the involvement of sharp-wave ripples (SWR, 100 to 200 Hz), a property of the CA3–CA1 network (Buzsáki 2015) mostly salient during NREM sleep. In fact, (1) SWRs support the replay of neural ensembles that have been engaged in memory encoding (Foster and Wilson 2006; Peyrache et al. 2009), (2) the suppression of SWRs during sleep impairs memory performance (Girardeau et al. 2009; Maingret et al. 2016), and (3) SWRs are coupled to the active, up-state of slow oscillation (SO; <1 Hz) in specific associative areas in the neocortex (Sirota et al. 2003; Battaglia et al. 2004).

Another "spontaneous" oscillatory component observed in the cortex during NREM periods are sleep spindles (Siapas and Wilson 1998; Ngo et al. 2020). These events are waxing and waning oscillatory (8 to 16 Hz) bouts generated in the thalamus, triggered by the depolarizing inputs generated by cortical up-states (Timofeev and Steriade 1996). These events are also thought to be a component of memory consolidation across different species (Johnson et al. 2010; Latchoumane et al. 2017; Cowan et al. 2020; Xu et al. 2021), and they tend to co-occur with the hippocampal SWRs (Siapas and Wilson 1998; Ngo et al. 2020) as well as the up-state of the SO on the cortical surface of associative areas (Andrade et al. 2011; Niethard et al. 2018; Ngo et al. 2020; Staresina et al. 2023). Taken together, this evidence suggest that the SO–spindle–SWR loop may orchestrate neural plasticity across various regions and contribute to the process of memory consolidation (Staresina et al. 2015; Maingret et al. 2016; Niethard et al. 2018).

SWRs do not interact uniformly with all cortical areas: the Default Mode Network (DMN) is a resting-state network, which, among other functions, has been implicated in memory processes (Buckner et al. 2008; Tambini et al. 2010). Recently, combining electrophysiology in the hippocampus with brain Blood Oxygen Level Dependent (BOLD) activity, Kaplan et al. reported that primate SWRs were strongly related to a pattern of activity including large portions of the DMN (Kaplan et al. 2016). This result has also been confirmed in mice, on a finer time scale with wide-field voltage imaging (Karimi Abadchi et al. 2020; Pedrosa et al. 2022a). In rodents, the DMN comprises areas such as the orbitofrontal, anterior cingulate, retrosplenial, parietal, temporal association cortex, and the dorsal hippocampus (CA1; Lu et al. 2012). Studies investigating the functional connectivity between SWRs and these DMN regions have shown a diversity of spatiotemporal patterns, suggesting the existence of multiple modes of interactions between SWRs and the cortex (Oliva et al. 2016; Wang and Ikemoto

Received: November 23, 2023. **Revised:** February 13, 2024. **Accepted:** February 14, 2024.

2016; Karimi Abadchi et al. 2020; Opalka et al. 2020; Nitzan et al. 2022; Pedrosa et al. 2022a).

Resting-state networks are typically studied with transcranial electrophysiology (EEG) and functional magnetic resonance imaging. However, these noninvasive approaches, commonly used for studying human brain activity, cannot offer the spatiotemporal resolution needed to unveil the mechanistic underpinnings of information processing. To investigate the relationship between DMN activity and hippocampal SWRs, here we analyze recordings (Pedrosa et al. 2022a) in anesthetized mice, combining (1) wide-field voltage-sensitive dye (VSD) imaging and (2) a transparent wide-field electrocorticography grid (ECoG) from the neocortex and (3) local field potential (LFP) from the ipsilateral CA1 hippocampus. We discovered different cortical patterns of SO within the DMN and across the dorsal cortex, and we studied them in the context of their interaction with hippocampal SWRs during NREM sleep. Interestingly, we found that a specific cortical pattern centered around the retrosplenial cortex (previously reported by Karimi Abadchi et al. 2020) is topographically matched by the spatial distribution of cortical spindles. Using a complementary dataset of mice during natural sleep, we found that both SO and spindle transients in the retrosplenial cortex are correlated with slow gamma (20 to 45 Hz) in CA1 *stratum radiatum*. Combined SO–spindle transients observed in the retrosplenial cortex tend to precede hippocampal SWRs, suggesting that the retrosplenial cortex is a hub of spontaneous activity processes during sleep, potentially playing a key role in memory consolidation.

Materials and methods

The dataset used in this study was previously published in Pedrosa et al. (2022a).

Animals

For acute VSD imaging (urethane group), five C57/Bl6 adult male mice (ages 2 to 4 months) were used. Under a 12-h light/dark cycle, the animals were housed in conventional plastic cages with other animals. Water and food were available to the animals at all times, ad libitum. The Animal Welfare Committee of the University of Lethbridge accepted the animal experimental methods and followed all of the standards set out by the Canadian Council on Animal Care. They were given a pulse of electrical, tune, or light stimulation to map different sensory cortices.

For voltage-sensitive imaging (VSI), five CaMK2A-tTA;tetO-chiVSFP mice (male, 3 to 6 months old) were used, weighing between 25 and 35 g. To protect the implants, the animals were housed in groups until surgery day, then separately afterwards. For this group, all the experiments were conducted during the light period. The Central Commission Dierproeven and the Radboud University Animal Welfare Board approved this experimental technique, which was carried out in compliance with the Experiments on Animals Act and the European Directive 2010/63/EU on animal research.

Surgery

Surgical preparation for the VSD imaging

First, mice were anesthetized with 3% isoflurane with 100% of oxygen and sedated with urethane (1.25 mg/kg). The animals were subsequently placed in a stereotaxic apparatus and kept under 0.5% to 1% isoflurane anesthesia using a nasal mask. A heating pad controlled by a feedback thermistor kept the body temperature at 37°C. To reduce discomfort, 80 mg of dexamethasone was given intramuscularly. Following previous protocols (Karimi Abadchi et al. 2020; Pedrosa et al. 2022a; Pedrosa et al. 2022b), two Teflon-coated stainless-steel wires (277 m diameter) were inserted as ground on the pial surface of the cerebellum and in the hippocampus (−4.3 mm AP and +2.4 mm ML, +1.8 mm DV at a 60-degree angle) for hippocampal recordings. Cyanoacrylate glue and acrylic resin were used to secure the electrodes to the skull. Next, a tracheostomy was performed to aid the animal's breathing. For skull removal, a unilateral craniotomy window was created. Following the craniotomy, the exposed cortex was fully covered with 4-(2-hydroxyethyl)-1-piperazineethanesulfonic acid (HEPES)-buffered saline solution (1 mg/ml) and administered to preserve hydration.

Surgical preparation for the VSI group

Animals were sedated with 2% isoflurane at 100% oxygen concentration, then placed in a stereotaxic apparatus and kept under 0.5% to 1.5% isoflurane via a nasal mask. A heating pad controlled by a feedback thermistor kept the body temperature at 37°C. At the start of the anesthetic, a subcutaneous dose of 5 mg/kg of carprofen was injected, followed by 50 μl of 2% lidocaine through the scalp. During the surgery, the levels of isoflurane and oxygen were monitored and regulated to keep the respiratory rate between 0.5 and 1.5 Hz. A skull screw was then placed above the left cerebellum to provide a shared reference and ground for the silicon probe. After that, two more skull screws were placed on the left hemisphere to help secure the head-plate implant. The exposed right hemisphere skull was next thinned to remove tiny skull capillaries in order to improve later voltage imaging recording. We performed a craniotomy on the pial surface of the right cerebellum (−4.3 mm AP and +2.4 mm ML) and inserted a 16-channel silicon probe with an inter-site pitch of 50 m (E16 R 50 S1 L10; Atlas Neuroengineering, Belgium) in the intermediate hippocampus (+2.1 mm DV at a 57-degree angle toward the back) for CA1 laminar recordings. The electrodes were carefully attached to the skull with cyanoacrylate. Finally, we used acrylic cement to attach a head-plate with a wide-field view of the right hemisphere to the skull (Super-Bond C&B). All animals were given at least 4 days after surgery to begin acclimating to the arrangement. For a complete description of the protocol, see Pedrosa et al. (2022b).

VSD imaging recordings

After the surgical procedure, RH1961 was dissolved in 0.5 mg/ml HEPES-buffered saline and administered to the exposed cortex for 40 to 60 min. After that, 1.5% agarose in HEPES-buffered saline was applied over the cortex and sealed with a coverslip to minimize respiration artifacts. Using a charge-coupled device (CCD) camera (1 M60 Pantera, Dalsa, Waterloo, ON) and an EPIX E8 frame grabber controlled by XCAP 3.7 imaging software (EPIX, Inc., Buffalo Grove, Illinois) and XCAP 3.8 imaging software (EPIX, Inc.), VSD images were acquired in 12-bit format at a frame rate of 200 Hz (EPIX, Inc.). Images were captured using a macroscope with front-to-front video lenses (8.6 × 8.6 mm field of view, 67 μm per pixel). Two LEDs (627-nm center; Luxeon K2) were used to excite the VSD, and the fluorescence emitted was filtered through a 673-nm to 703–29-nm bandpass emission filter. To characterize the neocortical topography, we applied the same sensory stimulation previously described by Mohajerani (Mohajerani et al. 2013; Karimi Abadchi et al. 2020) to localize different primary sensory areas (HLS1: hindlimb, FLS1: forelimb, V1: visual cortex) in order to inspect the local evoked activity in the VSD data.

VSI recordings (natural sleep)

Two synchronized scientific Complementary Metal-Oxide-Semiconductor (sCMOS) cameras (PCO edge 4.2) operated by a transistor-transistor logic (TTL) external trigger and coupled

with a Leica PlanAPO1.6 lens were used to capture wide-field epifluorescence. The excitation light was provided by a high-power halogen lamp (Moritex; Brain Vision) installed in the macroscope. As optical filters, we used mCitrine emission FF01-542/27, mCitrine excitation 500/24, mKate2 emission BLP01-594R-25, and beam splitters (515LP, 580LP). The image was captured at 375 × 213 pixels (spatial resolution of ∼36 μm/pixel; 12-bit) at 50 Hz in 15-min blocks.

Electrocorticography grids

The fabrication of the PEDOT:PSS ECoGs (Fig. S1D) has been described previously (Khodagholy et al. 2013; Donahue et al. 2018) and consisted in the deposition and the patterning of parylene, metal, and PEDOT:PSS. First, a 3-μm-thick parylene-C film was deposited on top of a glass slide using a SCS-Labcoater 2. Metal pads and interconnects were patterned by lift-off using S1813 photoresist exposed to UV light with a SUSS MBJ4 mask aligner and developed with MF-26 developer. Chromium (5 nm) and gold (150 nm) were deposited with a thermal evaporator, and the final pattern was obtained by lifting the resist in a mixture of acetone and isopropanol. A second 3-μm-thick layer of parylene was used to insulate the metal tracks, followed by the deposition of a soap solution (4%wt) and a third "sacrificial" 3-μm-thick layer of parylene. They were patterned using AZ9260 photoresist and reactive ion etching with an oxygen plasma using an Oxford 80 plus, leading to openings on the electrodes (20 μm × 20 μm) and the contact pads. Twenty milliliters of PEDOT:PSS (Clevios PH 1000) was mixed with ethylene glycol (5 ml) and dodecyl benzene sulfonic acid (50 μl) to improve the conductivity and 3-glycidoxypropyltrimethoxysilane (0.25 g) to prevent film delamination. The solution was spin-coated on the glass slides and the sacrificial layer of parylene was removed by peel-off to leave PEDOT:PSS only on contact pads and electrode openings. Finally, the samples were baked at 140°C for 1 h to anneal the PEDOT:PSS films then immersed in water to remove excess of PSS in the PEDOT:PSS and release the ECoGs from the glass slides.

CA1 LFP and ECoG recordings

We employed a transparent ECoG grid to obtain an electrophysiological profile of the neocortex. The recording sites on the grid are grouped in a 6 × 5 matrix (each site is spaced 1 mm apart) and cover a total area of 6 mm × 5 mm. To capture neocortical activity, we first grounded the grid to the animal's nose with a subcutaneously implanted electrode. The ECoG matrix was then placed across the mouse's right neocortex, encompassing the same wide field as the optical imaging. After that, we applied HEPES-buffered saline to the exposed cortical region to keep it hydrated. The electrophysiological data were captured using 32-channel headstages (Intan Technologies' RHD2132) coupled to an Open Ephys recording system. The raw signals were recorded at 20-kHz sampling rate and filtered between 0.1 and 7500 Hz with a pre-amplification of 20×.

For the VSD recordings, we recorded the hippocampus LFP at 20-kHz sampling rate in a Digidata 1440 (Molecular Devices Inc., California) data recording system, with a Teflon-coated stainless-steel wire. The recorded data were filtered (0.1 to 10,000 Hz) using a Grass A.C. Model P511 (Artisan Technology Group, Illinois). For the VSI recordings, instead, we used a 16-channel silicon probe (Atlas Neuroengineering, Belgium). The CA1 profile data were acquired using headstages (RHD2132; Intan Technologies) with an Open Ephys system. The signals were recorded at 20-kHz sampling rate and filtered between 0.1 and 7,500 Hz.

Voltage imaging preprocessing

For the VSD imaging preprocessing, we used methods as detailed elsewhere (Karimi Abadchi et al. 2020; Nazari et al. 2023). We first applied a high-pass Chebyshev filter above 0.2 Hz to the time series of each individual pixel. Next, we averaged the filtered signal of each pixel and defined it as the baseline signal (F_0). The filtered signal was then subtracted by the F_0, and the resultant difference was divided by the F_0 values ($F - F_0/F_0 \times 100$). For the VSI recording and preprocessing details, we repeated the protocol previously reported (Song et al. 2018; Pedrosa et al. 2022a; Pedrosa et al. 2022b).

Ripple detection

We initially downsampled the data to 1 kHz and filtered in between 150 and 300 Hz. After, we detected the peaks of the envelope filtered data that crossed a threshold between 3 and 5 SD plus the mean. Based on the points that crossed 1.5 SD before and after the detected points, the start and end of the ripple were determined. Events with length longer than 30 ms and shorter than 300 ms were considered ripple events. In addition, the time between the end of one ripple and the beginning of the next had to be at least 100 ms.

Spindle detection

We filtered the raw signal from each ECoG channel in the 8- to 16-Hz band, computed the power of the resulting signal, and z-scored it. For each channel, we defined the presence of significant spindle power whenever this score exceeded the value of 2. We then defined a measure of global spindle power activity as the number of simultaneously "active" ECoG channels at any moment in time. Finally, we classified spindle events as time windows in which the number of active channels exceeded the average value computed on the entire recording session. We rejected events shorter than 200 ms. For each of these events, we then computed a size score as the cumulative sum over the duration of the event, of the number of active channels per time bin. A similar measure was also computed for each channel separately, as the number of time bins within an event in which that particular channel exceeds the spindle detection threshold.

We then correlated the appearance of spindle events in the cortex with the presence of activity in specific frequency bands in the hippocampus. Hippocampal LFP was filtered in separate frequency bands: spindle (8 to 16 Hz); gamma (25 to 50 Hz); ripple (150 to 250 Hz). Next, we computed the power in time for each of these bands. To obtain an estimate of the ripple power density, the ripple time series was also smoothed with a large temporal kernel of 100 ms.

The temporal alignment between cortical and hippocampal oscillatory events was evaluated by normalizing the length of all spindle events to a time window of equal length and subsequently computing the correlation between the size of each aligned spindle event and the hippocampal power detected at different lags with respect to the onset and offset of the spindle event. In particular, we computed the correlation of gamma power versus spindle size and ripple power versus spindle size. In both cases, we factored out the contribution of the spindle band in the hippocampus (a potential confounding factor due to volume conductance between cortical recording sites and the hippocampus) by computing a partial correlation of the aforementioned factors. Such correlations were computed both considering the overall size of the cortical spindle event (thus including all ECoG

channels) or separately by considering the presence of spindle-related activation in each of the channels separately.

Spindle power

Spindle power was defined as the envelope of the filtered raw data (8 to 16 Hz) in each individual channel. In order to avoid problems with the different impedance across electrodes, the resultant signal was z-scored for each individual channel.

Register multimodal images

To establish a unified spatial framework for the cortical images encompassing all mice, we utilized the imregister function from the Image Processing toolbox (https://nl.mathworks.com/products/image.html) from MATLAB (MathWorks). This function used an intensity-based algorithm to automatically align images to a shared coordinate system, improving comparability across all subjects. Our approach involved systematically re-spacing all acquired images for each animal to a common anatomical mask.

The image registration process employed a multimodal registration configuration, with careful adjustments to parameters for optimal performance. Specifically, we configured the initial radius parameter (to 3.5) to ensure precise alignment. In addition, the "Affine transformation model" was chosen as the registration method to facilitate accurate spatial correspondence. The anatomical mask used as the reference point was meticulously crafted through manual delineation using ImageJ, utilizing cortical images from mouse 1.

Results

Experimental design for the spatiotemporal investigation of the neocortex during SWR event

To investigate patterns of neocortical activity during hippocampal SWRs using wide-field VSD imaging and electrophysiology, we developed a novel electrocorticography grid (Fig. 1A and B) (ECoG; 6 × 5 matrix with a pitch of 1 mm between the electrodes) based on a conformable and transparent parylene-C substrate and a mixed organic ionic/electronic conductor, poly(3,4-ethylenedioxythiophene):polystyrene sulfonate (PEDOT:PSS). PEDOT:PSS is commonly used to lower impedance of metallic electrodes, typically by one order of magnitude (Sessolo et al. 2013), leading to higher signal-to-noise ratio (SNR). The impedance of our electrodes was ∼20 kΩ for electrodes of 20 μm × 20 μm (Fig. S1). PEDOT:PSS-based ECoGs have been used on top of the brain to record LFPs and even action potentials in rodents and humans (Khodagholy et al. 2013; Khodagholy et al. 2015; Khodagholy et al. 2016). Higher SNR also means that we can use smaller electrodes, which, combined with the transparency of the substrate, leads to a better optical imaging due to less shadow from the electrodes in the field of view (Donahue et al. 2018). The ECoG was designed to cover the entire cortical area recorded (Fig. 1C).

Using a similar experimental protocol developed previously by Mohajerani and colleagues (Karimi Abadchi et al. 2020), which combined VSD imaging (Bermudez-Contreras et al. 2018; Kyweriga et al. 2017; Mohajerani et al. 2013) and electrophysiology in the dorsal hippocampus of mice under urethane anesthesia (Fig. 1D to G), we expanded on this setup by further adding a transparent ECoG matrix. This addition allowed us to better capture both cortical SOs and cortical spindles in a high spatiotemporal resolution. The resulting dataset has been already used for the study published in Pedrosa et al. (2022a). Here, we extend the analysis of the sleep-like state induced by anesthesia to address different aspects of cortico-hippocampal activity, focusing particularly on the interaction between hippocampal SWRs and cortical oscillatory activity at different sites.

Hippocampal SWRs in mice are associated with default mode network activity at different temporal scales

First, we investigated the spatiotemporal activity in the neocortex in correspondence with detected SWR events (150 to 300 Hz) in the hippocampal CA1 region. As previously reported, at the time of SWR appearance, cortical areas participating in the DMN became active (Fig. 2A; Video 1) (Kaplan et al. 2016; Karimi Abadchi et al. 2020). In particular, activation was observed in areas along the midline, namely, retrosplenial (RS) and anterior cingulate (AC) cortices, together with a lateral complex of areas including primary auditory cortex and temporal association cortex (A1/TeA) (Fig. 2B). This pattern was consistently present across mice in the dataset (Fig. 2C). As the proximity between AC and secondary motor cortex makes it difficult to resolve these two areas with our technique, we referred to this area as M2/AC (Mohajerani et al. 2013; Karimi Abadchi et al. 2020).

Although peak activations of RS, A1/TeA, and M2/AC around the hippocampal SWRs are significantly correlated (Fig. 2D; total: 2,718 SWRs detected; R: between 0.22 and 0.33 and P: between 1.0421e-30 and zero for all comparisons, using Spearman's rank correlation), there is considerable variability across events and areas, suggesting that DMN responses to SWRs may be more diverse than previously reported (Karimi Abadchi et al. 2020; Pedrosa et al. 2022a).

Multimodal default mode network activation around SWRs

To investigate the dynamics of cortical DMN areas around the hippocampal SWRs, we used unsupervised classification to find the canonical cortical activation modes that accompanied hippocampal SWR events. First, we applied register multimodal images on the cortical activity (averaged from −0.2 to 0.2 s) for all the detected SWRs to apply a common mask (Fig. 3A) and align data from multiple animals. Next, we used a combination of principal component analysis (PCA) followed by independent component analysis (ICA) to extract the components best describing the cortical spatial patterns of activation around SWRs (Fig. 3B; Lopes-Dos-Santos et al. 2018; Lopes et al. 2013). Firstly, it was clear from the unimodal distribution of scores that it was not possible to classify SWRs into different families based on the associated cortical activation. Nevertheless, one could still ask how each component modulated the activation of specific cortical areas. Indeed, we observed that DMN broke into separate subnetworks, each corresponding to high (top 10%) activation of a different component (Fig. 3C). This effect was independent of the number of extracted ICA components (Fig. S2) and indicated the presence of a diversity in the cortical correlate of SWRs, spanning a continuum between complementary patterns of activation.

Namely, IC1 and IC2 delineated a partition of the DMN between the activity of a RS–M2/AC complex and A1/TeA. So far, only patterns compatible with IC1 have been reported to occur during sleep (Karimi Abadchi et al. 2020; Pedrosa et al. 2022a). IC3 showed instead a generalized inhibitory pattern across multiple cortical areas. We next investigated how the properties of SWR events varied according to the corresponding values of the cortical ICA scores. Interestingly, we found a significant correlation between score of the ICA and ripple amplitude for IC2 and IC3, while for IC1 we found a significant correlation with the ripple duration

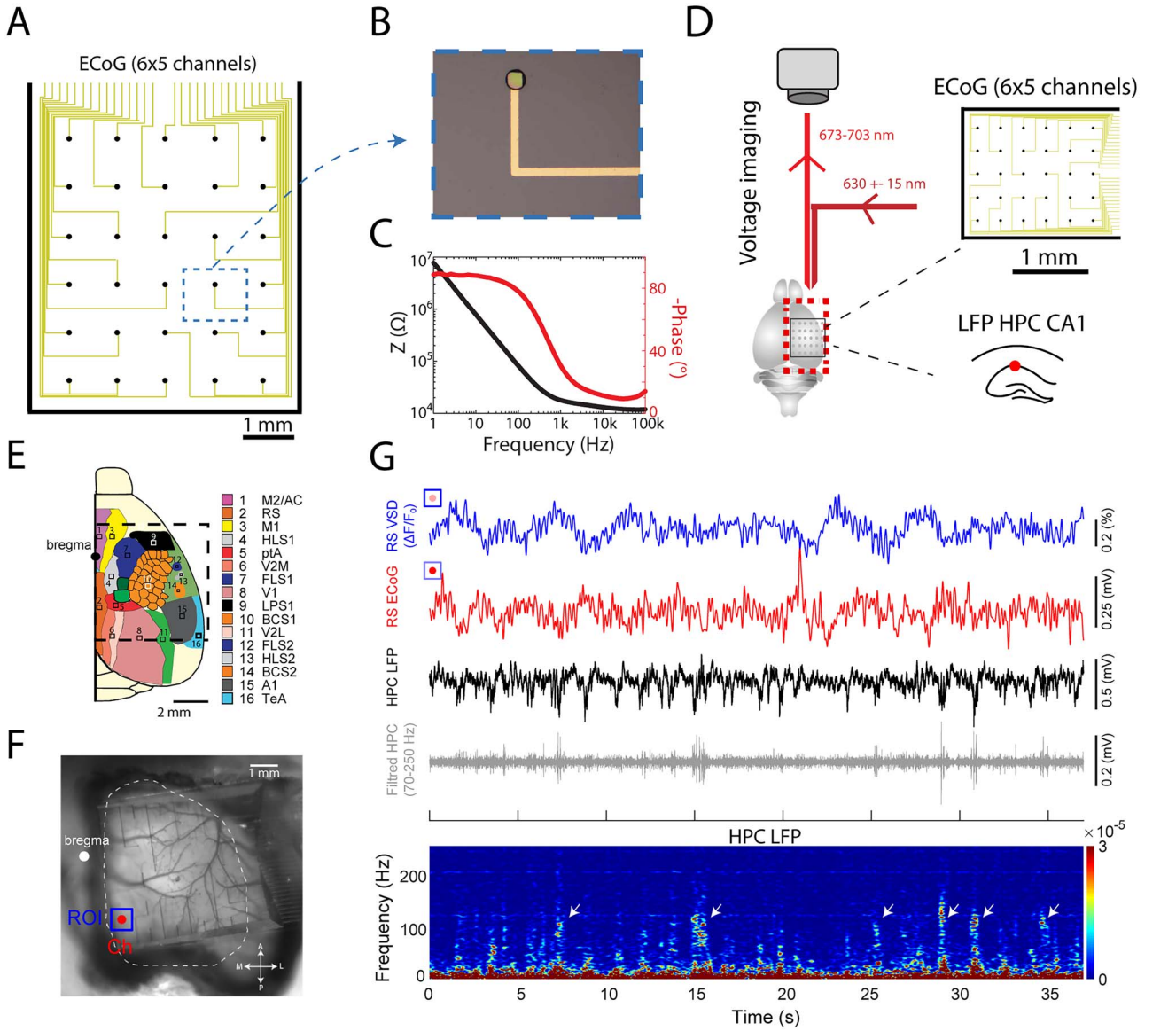

Fig. 1. Experimental setup used for recording the neocortical activity around SWRs. **A**) Schematics of the 30-channel ECoGs. **B**) Magnified image of 20 μm^2 × 20 μm^2 electrode covered with PEDOT:PSS. **C**) Electrochemical impedance magnitude and phase of a single electrode. At 1 kHz, the impedance is about 20 kΩ. **D**) Schematics of the experimental setup used for combined neocortical optical imaging, hippocampal LFP, and electrocorticography. The VSD imaging was performed using a CCD camera. Ipsilateral LFP of the dorsal CA1 was recorded from a single electrode implanted from the posterior region of the scalp. A neocortical LFP was also recorded from a transparent grid of electrodes (6 × 5 channels). **E**) Illustrative neocortical topographical map of brain area included in wide-field optical imaging. The dashed line represents the boundary of the imaging window. Bregma is represented as a dot in the midline. **F**) Photograph of a wide unilateral craniotomy with the transparent ECoG grid. The dashed contour renders the extent of the neocortex. Bregma is depicted as a dot. Axes: anterior (A), posterior (P), medial (M), and lateral (L). The red dot is an ECoG recording site on the retrosplenial cortex and the blue square is a region of interest (ROI) selected around this channel (Ch). **G**) Example of the optical and ECoG signals from the retrosplenial cortex selected from the ROI and recording site shown in (**F**). Note that both activities have a similar oscillatory pattern. Both VSD and ECoG signals are filtered between 0.2 and 6 Hz. Below, aligned hippocampal LFP (black) and filtered hippocampal LFP (gray, 70 to 250 Hz). Bottom, the spectrogram of the hippocampal LFP shows peaks of high-frequency oscillation.

($n = 2{,}718$, $^*P < 0.05$; Fig. 3E). We did not find a significant correlation with ripple frequency. Together, these findings indicate that features of SWR events might correlate with specific parts of DMN activity.

Although the number of SWRs varies across mice (mouse 1 = 177/0.1 Hz, mouse 2 = 669/0.12 Hz, mouse 3 = 1,000/0.14 Hz, mouse 4 = 423/0.08 Hz, and mouse 5 = 449/0.09 Hz; total = 2718), the distribution of SWR events dominated by each cortical IC for each animal was similar (Fig. S2B and Fig. 3F). To measure this SWR event distribution, we subdivided SWR events into three groups based on their IC scores. Using data from all mice, we identified SWR events occupying different portions of the score space by taking the 10% of SWRs expressing the top 10% score values for each IC (Fig. 3B, Fig. S2B; distribution of events per cluster: Cluster1 = 42%, Cluster2 = 26%, and Cluster3 = 32%). The events classified in each group (equivalent to the ICs from Fig. 3C) were then reassigned to the respective mouse (Fig. 3F).

Co-occurring SWRs and RS activation predict spindle bouts

Although, as shown above and previously in the literature (Siapas and Wilson 1998; Battaglia et al. 2004; Peyrache et al. 2011),

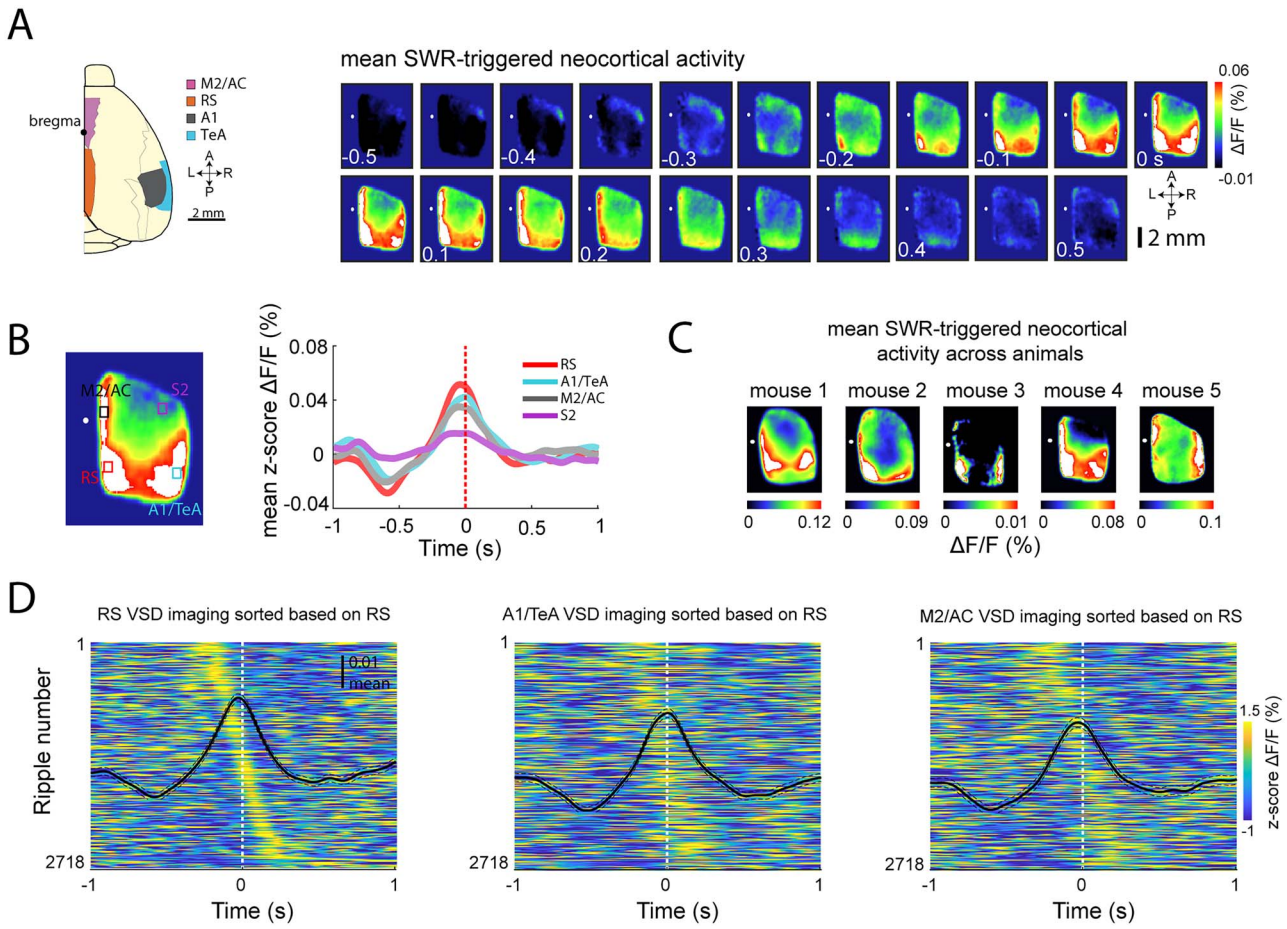

Fig. 2. DMN areas activate differentially around hippocampal SWR. **A**) Mean cortical voltage imaging signal around SWR events. The dot represents the bregma position. **B**) On the left, the averaged cortical activity around SWR (between −100 and 100 ms) from the example in (**A**). The selected areas are retrosplenial (RS), secondary motor and anterior cingulate (M2/AC), secondary sensory (S2), and primary auditory and temporal association area (A1/TeA). For each mouse, we determined the ROI based on the evoked activity area from the stimulation data and the topographic map (see Materials and Methods). On the right, the averaged activity across animals of areas shown on the left panel ($n = 5$ mice). **C**) Averaged cortical activity (between −100 and 100 ms) for each individual mouse. Note for all the mice the high activity of the DMN areas (mouse 4 is the animal from the example in (**A**)). **D**) Aligned RS, A1/TeA, and M2/AC activity around all the detected SWR events. The plots are sorted by the RS activity.

SWRs, sleep spindle, and slow oscillations have a tendency to co-occur, little is known about the spatiotemporal features of their interaction. To characterize this relation, we used the ECoG data to analyze the sleep spindle activity around the SWR during the different cortical IC clusters (Fig. 4A).

Taking the 10% of the events with the highest weight for each IC, we observed that the overall spindle power is significantly higher for IC1 compared to IC2 and IC3 (Fig. 4B; one-way ANOVA, *P*-values: 10% = 0.04; one-way *t*-test compared to zero, *P*-value: 10% = IC1/0.001, IC2/0.61, and IC3/0.92). Extending the range of included events to 15% and 20%, therefore including events that are increasingly poorer representatives of each IC, still resulted in a significant (although weaker) effect for IC1 (Fig. S3D; 15%: IC1 $P = 0.003$, IC2 $P = 0.38$, and IC3 $P = 0.78$; 20%: IC1 $P = 0.004$, IC2 $P = 0.14$, and IC3 $P = 0.75$).

More specifically, we found that spindle activity around IC1 peaks also coincided with the topographic profile of the related IC (Fig. 3D and Fig. 4B).

In order to provide a concrete connection between the IC profiles and spindle activity, we then took advantage of the higher temporal resolution power of the ECoG signal to disentangle contributions in different frequency ranges to the overall cortical activation. We fit a generalized linear model (GLM) to detect the spatial patterns of spindle activity associated to each SWR's IC (Fig. 4C). We used the IC scores of each SWR event as regressors to predict the spindle power simultaneously recorded on a ECoG contact point. We repeated the same procedure over the entire set of ECoG array contacts, thus obtaining a mapping of the relative influence of the IC modulation on the observed spindle power at different cortical locations. In contrast to IC2 and IC3, which showed almost no significant coupling to spindle power, IC1 presented significant weights in relation to the electrodes that occupied the region around RS. To specify this result as a property of the spindle frequency band, we also repeated this analysis but predicting cortical slow gamma (20 to 45 Hz) and medium gamma (60 to 90 Hz, Fig. S3A). As opposed to spindle activity, neither gammas showed significant couplings with IC scores, nor clear spatial organization (Fig. S3B), thus suggesting that cortical activation associated with SWRs with high IC1 scores is mostly driven by spindle events in the RS area.

Next, we asked how the overall variability and dynamical range of cortical spindle activity related to that linked to hippocampal SWR time intervals. We used the same previously applied PCA/ICA decomposition approach to the spatial map of spindle power obtained from the ECoG (Fig. 4D; Fig. S3C). In doing so, we obtained a new and independent set of independent components (spindle independent components, sIC) describing the direction of co-variability in spindle spatial organization. Interestingly, sIC

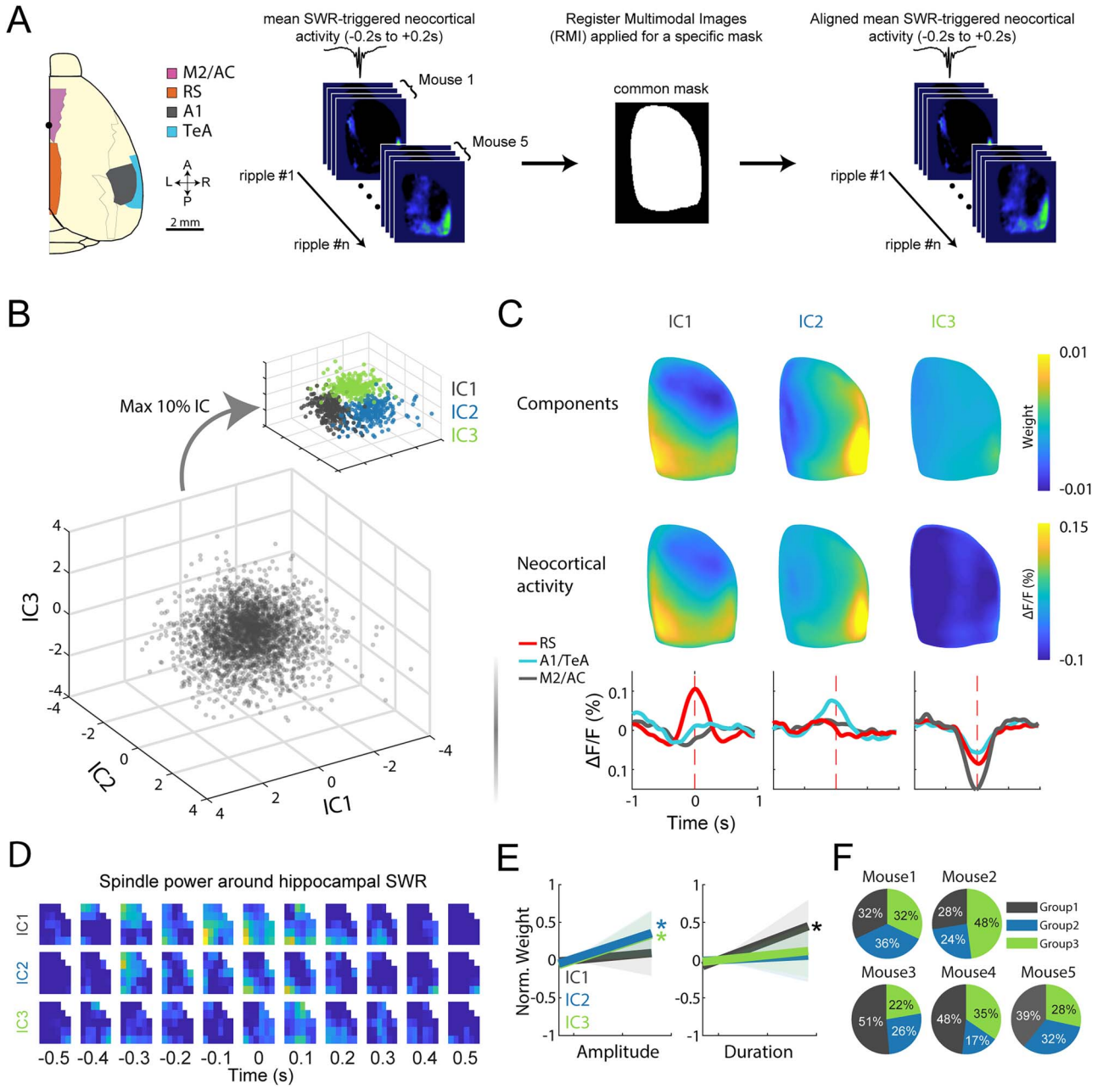

Fig. 3. DMN has distinct cortical activity patterns around hippocampal SWR. **A**) Schematics of the pipeline used to merge data across animals. For the cortical map characterization, we averaged the cortical imaging data between −0.2 and 0.2 s around each detected SWR. **B**) Scatter plot shows the first three estimated independent components of the cortical activity for each detected SWR ($n = 2{,}718$ from 5 mice). Each color represents the 10% events with the highest weight for each component. **C**) ICA components (top) and the averaged neocortical activity from the 10% of the events with the highest weight for each IC (middle). On the bottom, we show the time evolution of RS, A1/TeA, and M2/AC from the averaged events showed in the middle plot. **D**) Spatiotemporal spindle power for each IC. The averaged events are the events with the highest weight for each IC (20% highest events). **E**) SWR information for each IC. The bars show the correlation between the weight in each IC with the amplitude and duration of the ripple events (*$P < 0.05$). **F**) Probabilistic distribution of the 3 clusters for each individual mouse.

showed a similar profile found in the VSD data (IC). Correlating the scores from the sIC components with the cortical ICA components, we observed a one-to-one correspondence between the two sets of ICs. However, this relationship was not consistently significant (Fig. 4D).

Cortical spindles in retrosplenial cortex correlate with CA1 slow gamma activity during the SWR

In a previous study analyzing the same data as here, we have shown that RS activation is connected to slow gamma (20 to 45 Hz) oscillations in the CA1 during NREM sleep (Pedrosa et al. 2022a). Furthermore, this interaction could also be observed with slow gamma bouts simultaneous with SWRs. This led us to ask whether cortical spindles also participate in this retrosplenial–hippocampal interaction during ripples. To measure how hippocampal slow gamma interacts with cortical spindles during SWRs, we computed the cross-correlation between slow gamma power during SWRs with the spindle power in each ECoG channel around the ripple (Fig. 5A). We calculated this correlation multiple times, one for each IC, by using only the 10% of SWR events

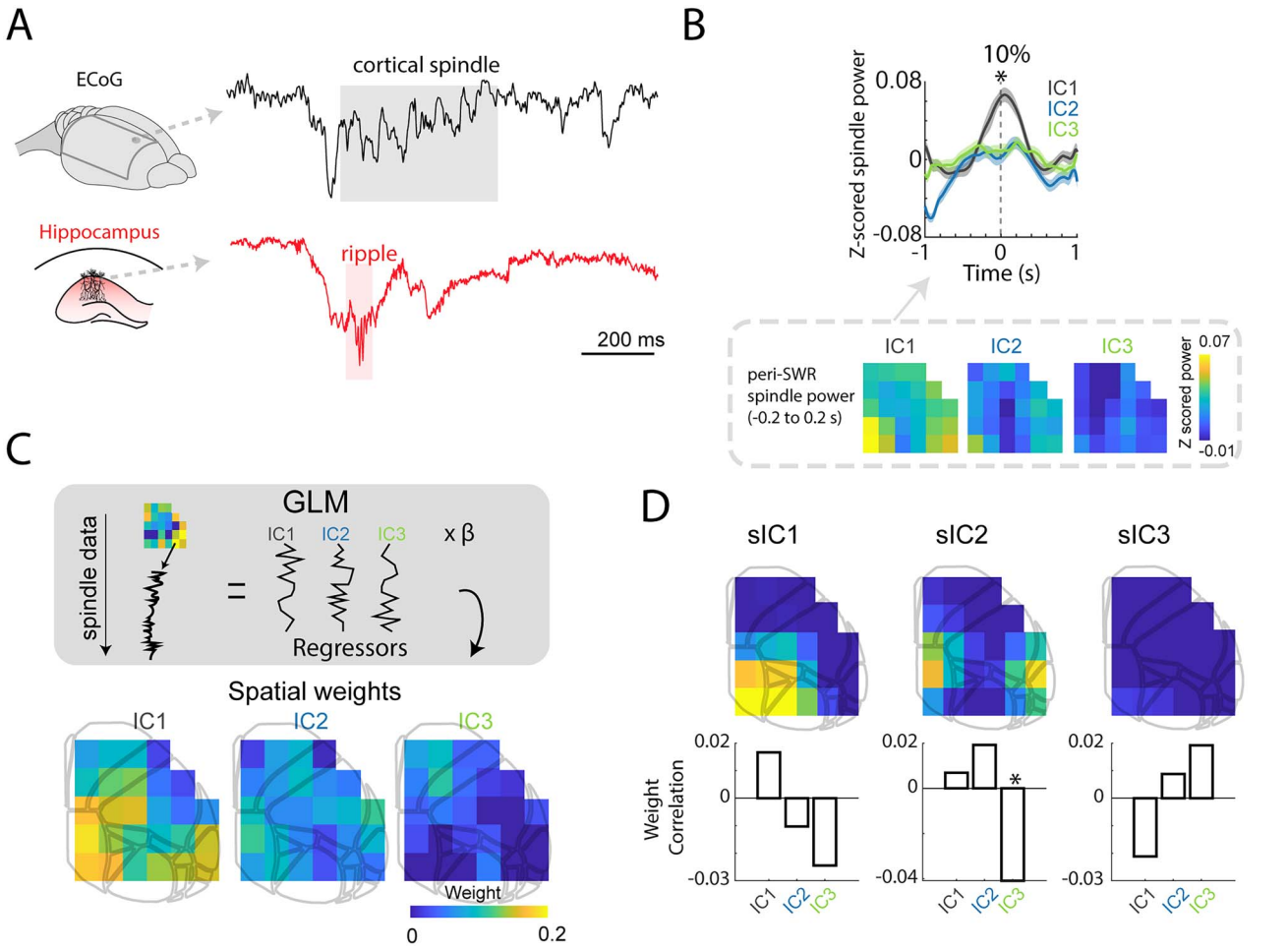

Fig. 4. Cortical spindle coactivate with SO in RS around hippocampal SWR. **A**) Example of a SWR event detected in the hippocampus coupled with a cortical spindle detected in a frontal electrode from the ECoG. **B**) On top, the global spindle power (8 to 16 Hz) averaged between −1 and +1 s around the SWR for each IC. Each line represents the mean activity of all the electrodes averaged only on 10% of events with the highest weight for each IC (one-way ANOVA, *$P < 0.05$). On the bottom, spatial distribution of the spindle power around −0.2 to 0.2 s for the 10% cluster. **C**) Spindle power data for each SWR were fitted with the IC weights as parameters in a GLM to observe the predominance of the spindle power in each electrode for the IC clusters. **D**) IC components from the spindle power data around the SWRs (averaged −0.2 to 0.2 s). The bars are the correlation r values between the weights from the sIC (ECoG) and the IC (VSD) (*$P < 0.05$).

with the highest weight for each IC. We observed a significant correlation between the ECoG channel located around RS with the IC1 group of SWR events ($R = 0.035$, $P < 0.002$) in the 100 ms preceding the ripple peak (Fig. 5A). Interestingly, this correlation between RS spindles with CA1 slow gamma peaked before the ripple appearance. We did not find a significant result for IC3 and only a marginally significant site for IC2. This effect could not be observed when correlating ripple power with spindles (Fig. S4).

To confirm the relationship between slow gamma during SWRs and spindle power, we then subdivided all SWR events in four quantiles based on their associated slow gamma and ripple power. As expected, we observed the emergence of an association between the slow gamma component of the ripple and the simultaneous activation in the spindle range around RS (Spearman correlation, slow gamma $R = 0.97$, $P < 0.001$ and ripple $R = 0.026$, $P = 0.28$; Fig. 5B and C). We did not observe an equivalent modulation of spindle power when we considered the ripple component.

We then took the opposite perspective and analyzed this cortico-hippocampal interaction at the time of spindle events. For this, we detected cortical spindles and computed the correlation between hippocampal slow gamma and ripple power with the size of cortical spindle events. To minimize the influence of the volume conduction from the spindles, we performed partial correlations and factored out the contribution of the spindle frequency power (8 to 16 Hz) in the hippocampus. Interestingly, we found that the correlation between cortical spindles and slow gamma in the hippocampus showed significance during the entire duration of the spindle bout (Fig. 5D, $P < 0.01$). On the other hand, ripples only presented a small significant correlation on the period preceding the spindle. In particular, our results indicate that the correlation between cortical spindles and hippocampal slow gamma are spatially dominant on the cortical electrodes that overlap with the cortical DMN areas (Fig. 5E; Fig. S4B).

Finally, to investigate the CA1 source of this gamma activity, we used a second dataset combining wide-field VSI with a high-density silicon probe in CA1 in mice expressing genetically encoded voltage indicators (GEVIs) (Song et al. 2018). While this dataset did not include ECoG recordings (thus ruling out spindle-specific analyses), these recordings were performed during a state of natural sleep (Fig. 6A and B) and not under anesthesia. Repeating the same analyses of Fig. 3A to C on this second dataset, we confirmed results obtained under sleep-like state induced by anesthesia, and furthermore, we showed that the hippocampal

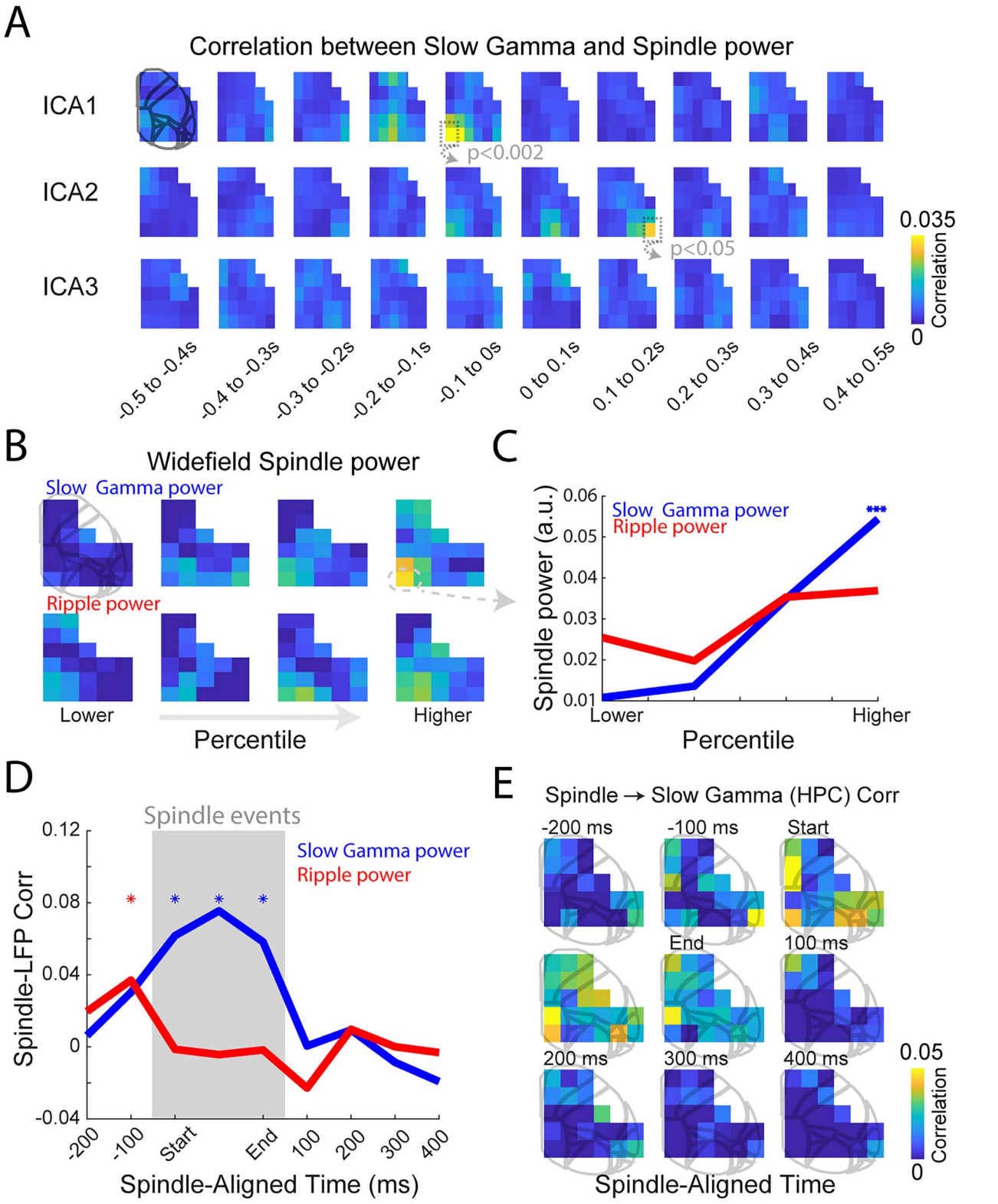

Fig. 5. Slow gamma during SWR is correlated to the spindle power in retrosplenial cortex. **A**) R values of the cross-correlation between hippocampal slow gamma power with the spindle power in each channel around the ripple events. The cross-correlation was computed with the averaged spindle power in a 100-ms window around the ripples. **B**) Averaged spindle power for four different quantiles of slow gamma and ripple power. **C**) Averaged slow gamma and ripple power in RS in different quantile sizes (Spearman's rank correlation coefficient, $^{***}P < 0.0001$). **D**) Temporal correlations between the overall amplitude of cortical spindle events and ripple and slow gamma power in the hippocampus, partialized by the power in the spindle frequency band in the hippocampus ($^{*}P < 0.05$). **E**) Same as (**D**) but considering the correlation of hippocampal activity in the ripple or gamma bands with spindle activity in single ECoG channels.

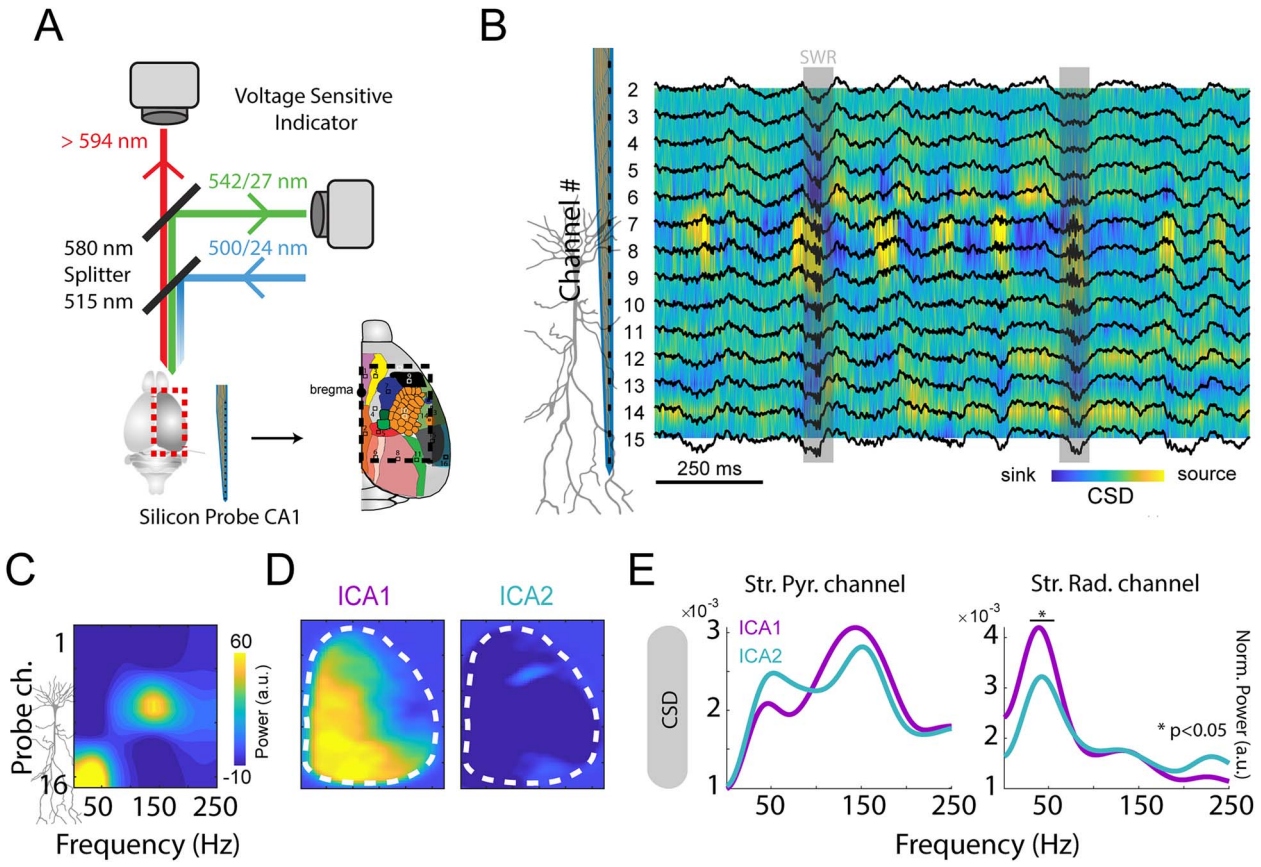

Fig. 6. Hippocampal slow gamma power is most strongly correlated with DMN activity during SWR. **A**) Illustration of the experimental setup used for the natural sleep recordings. In addition to the wide-field voltage imaging, we also implanted a high-density silicon probe (16 channels) in the hippocampus to record layer specific information in GEVI mice. **B**) Current-source density (CSD) signal computed from the silicon probe data in different CA1 layers during NREM sleep. **C**) Normalized power spectral activity across different CA1 layers for all the detected ripples. **D**) Cortical IC profiles calculated for the natural sleep recordings. Note we do not image A1/TeA in this dataset. **E**) Frequency amplitude in current-source density (CSD) from channels located in *Str. Pyramidale (pyr.)* and *Str. Radiatum (rad.)*. Note that no statistical difference was observed in ripple frequency band in *Str. Pyramidale*, while in slow gamma the IC1 was significantly stronger in *Str. Radiatum* (one-sample *t*-test $^{*} < P < 0.05$, $n = 5$).

slow gamma found to be associated with RS activity is located specifically in the *stratum radiatum* layer ($n = 5$ mice, Fig. 6C to E).

Discussion

Emergence of heterogeneous configurations within the default mode network during hippocampal SWRs

A basic tenet of the standard memory consolidation model is that the hippocampus encodes information and translates it to the neocortex (Marr et al. 1991; McClelland et al. 1995). Hippocampal SWRs are seen as critical for conducting this information to the neocortex and coordinating memory replays (Ji and Wilson 2007; Peyrache et al. 2009). Hippocampal SWRs and up-states tend to co-occur in the neocortex (Battaglia et al. 2004), particularly in areas associated with the DMN (Kaplan et al. 2016; Karimi et al. 2020; Pedrosa et al. 2022a). Parallelly, spontaneous cortical spindles transients (also located in the DMN) tend to precede SWR appearance (Siapas and Wilson 1998). But besides them being statistically synchronous, the precise spatiotemporal patterns of coordination of SO, spindles, and SWR have important implication for memory mechanisms (Geva and Nir 2019; Skelin et al. 2021).

The topography of SO and spindles in mice is not yet known with high resolution, partly due to limitations of recording techniques. Here, we combined wide-field voltage imaging and ECoG from the neocortex with the tracking of LFP activity in CA1, using mice during natural sleep or under urethane anesthesia (known as a good model of sleep) (Clement et al. 2008; Barthó et al. 2014; Greenberg et al. 2018; Pedrosa et al. 2022a). Voltage optical imaging offers significant advantages over classical approaches (such as MRI and electrophysiology): (1) temporal resolution comparable with electrophysiology and (2) no volume conduction.

Corroborating previous studies, our results also highlight the DMN as the network displaying the greatest modulation during and around hippocampal SWRs (Kaplan et al. 2016;Karimi Abadchi et al. 2020 ; Pedrosa et al. 2022a). However, we found that SWR events can coactivate separately with different subsets of DMN areas (Fig. 3). Using an independent component approach, we showed that DMN activation concentrates around two main hubs: medial (RS, AC, parietal, and secondary visual cortex) and lateral (A1, A2, and TeA). Previously, Lu et al. (2012) identified these two distinct subsystems within the DMN, describing the medial network (centered around RS) as a more hippocampal-related module and the lateral network as a "viscero-sensory" module due to the connection to multiple sensory modalities. In terms of functionality, one could speculate that these differences in activation across the DMN areas during SWRs may correspond to different information being reactivated and exchanged between the hippocampus and the cortex (Boyatzis et al. 2014). It is, therefore, possible that DMN activity configurations linked to different

SWRs might be associated to the consolidation of memories of distinct kinds.

Hippocampal SWRs correlate to RS "up-states" and spindle events

During sleep, RS cortex is one of the most strongly activated areas in correspondence to SWRs in the hippocampus (Karimi Abadchi et al. 2020; Pedrosa et al. 2022a). Comparing the features of SWR groups characterized by different cortical activation patterns, we found that those associated with a RS-centered activation had a longer duration. In fact, it has been shown that SWR size is associated to cortical spindles during sleep (Ngo et al. 2020). Consistently, we found that IC1, which strongly involves RS, is also the IC most correlated to spindle power (Fig. 4). On the other hand, IC3 showed an inhibitory pattern across multiple cortical areas. This behavior has been previously observed during awake SWRs (Abadchi et al. 2022). Here, we show that a fraction of sleep SWR are also related to cortical suppression, which includes spindle activity.

Thalamocortical spindles in RS around hippocampal SWR

Within the imaged regions in dorsal cortex, RS emerged as the cortical area with the highest spindle amplitude during the SWRs. Sleep spindles are produced by a corticothalamic feedback (Timofeev and Steriade 1996; Pinault 2004; Kim et al. 2015). Here, we hypothesize that RS cortex may play a prominent role in the interactions between this thalamocortical circuit and the hippocampus.

In humans, sleep spindles in the posterior cortex are commonly referred to as "centroparietal spindles" due to the fact that they are observed via EEG channels on the surface of the parietal lobe (Andrillon et al. 2011; Gorgoni et al. 2016; Cox et al. 2017). Nevertheless, as the primary source of brain activity expressed in EEG is cortical regions close to the scalp and its ability to measure brain activity originating in deeper brain regions is limited, finding the cortical origin of the spindle is challenging. However, activity from the RS (consisting of Brodmann areas 29 and 30, anatomically located deep in the parietal lobe; (Vann et al. 2009; Chrastil 2018) would topographically map onto the centroparietal region of the brain where human studies often observe spindles, suggesting that RS may be crucial for the spindles measured in the centroparietal region of the cortical surface.

Temporal relationship between RS and hippocampal activity around SWRs

Spontaneous neocortical activity during sleep statistically tends to organize in three functional networks (DMN, lateral network, and somatomotor network; Pedrosa et al. 2022a). Within the DMN cortical areas, RS cortex is a focus of activity initiation (Karimi Abadchi et al. 2020). Importantly, transient activations starting from RS cortex are associated with a greater increase in slow gamma power in the hippocampus, accounting to a large extent for the correlations between SWR and cortical activity. In addition, using a pseudo-causality analysis, Pedrosa et al. (2022a) also showed that in this RS–slow gamma (hippocampal) interaction, the neocortex tends to precede the hippocampus. In contrast, ripples precede widespread neocortical "up-state" across multiple areas (Nitzan et al. 2020; Tong et al. 2021; Pedrosa et al. 2022a). Together, these timing relationships (RS to slow gamma to ripple to cortex) describe a circular mechanism that may be fundamental for memory consolidation (Rothschild et al. 2017; Helfrich et al. 2019).

To investigate how cortical spindles may participate in this cortico-hippocampal dialogue, we first measured the correlation of hippocampal slow gamma power with the loadings of each ICs (Fig. 5A) and spindle power (Fig. 5B and C). Interestingly, we found not only a co-activation between RS spindle and slow gamma during SWR in the hippocampus, but also a tendency for RS spindles to precede SWR events. In general, spindle events were co-activating more with slow gamma than with ripples (Fig. 5D and E), suggesting that RS and the hippocampus could convey information through different oscillatory components and consequently various physiological mechanisms.

In conclusion, our work presented a novel picture of the cortico-hippocampal relationship unfolding during SWRs. Our results indicated that "up-states" and spindle activity localized in RS cortex can potentially modulate the sequential timing of multiple, spatially distributed events, organized around hippocampal SWRs.

Acknowledgments

The authors thank Thomas Knöpfel for donating the Butterfly 1.2 mice and for advice on imaging systems and preprocessing. The authors also thank Dr Jianjun Sun at the University of Lethbridge for the surgical assistance.

Author contributions

The project was conceived and designed by R.P., M.N., M.M., and F.B.; R.P. and F.S. analyzed the data; R.P. and M.N. performed surgery and electrophysiological recordings; L.K. and C.B. designed and manufactured ECoG grids; R.P. prepared the figures; R.P. and F.B. drafted the manuscript; R.P., M.M., L.K., C.B., F.S., and F.B. edited and revised the manuscript.

Supplementary material

Supplementary material is available at *Cerebral Cortex* online.

Funding

This work was supported by the Natural Sciences and Engineering Research Council of Canada (grant nos. 40352 and 1631465 to M.H.M.), Alberta Innovates (M.H.M.), Alberta Prion Research Institute (grant no. 43568 to M.H.M.), Canadian Institute for Health Research (grant nos. 390930 and 156040 to M.H.M.), National Science Foundation (M.H.M.), and European Commission grants ERC-AdG 833964 "REPLAY_DMN" (to F.P.B.), MSCA ITN 765549 "M-GATE" (to F.P.B.), and MSCA Intraeuropean Fellowship 840704 "Brownian-Reactivation" (to F.S. and F.P.B.).

Conflict of interest statement: None declared.

References

Abadchi JK, Rezaei Z, Knöpfel T, McNaughton BL, Mohajerani MH. Inhibition is a prevalent mode of activity in the neocortex around awake hippocampal ripples. *Elife*. 2023:12:e79513.

Andrade KC, Spoormaker VI, Dresler M, Wehrle R, Holsboer F, Sämann PG, Czisch M. Sleep spindles and hippocampal functional connectivity in human NREM sleep. *J Neurosci*. 2011:31(28):10331–10339.

Andrillon T, Nir Y, Staba RJ, Ferrarelli F, Cirelli C, Tononi G, Fried I. Sleep spindles in humans: insights from intracranial EEG and unit recordings. *J Neurosci*. 2011:31(49):17821–17834.

Barthó P, Slézia A, Mátyás F, Faradzs-Zade L, Ulbert I, Harris KD, Acsády L. Ongoing network state controls the length of sleep spindles via inhibitory activity. *Neuron*. 2014:82(6):1367–1379.

Battaglia FP, Sutherland GR, McNaughton BL. Hippocampal sharp wave bursts coincide with neocortical "up-state" transitions. *Learn Mem*. 2004:11(6):697–704.

Bermudez-Contreras E, Chekhov S, Sun J, Tarnowsky J, McNaughton BL, Mohajerani MH. High-performance, inexpensive setup for simultaneous multisite recording of electrophysiological signals and mesoscale voltage imaging in the mouse cortex. *Neurophotonics*. 2018:5(2):025005. https://doi.org/10.1117/1.NPh.5.2.025005.

Born J, Wilhelm I. System consolidation of memory during sleep. *Psychol Res*. 2012:76(2):192–203.

Boyatzis R, Rochford K, Jack A. Antagonistic neural networks underlying differentiated leadership roles. *Front Hum Neurosci*. 2014:8:114.

Buckner RL, Andrews-Hanna JR, Schacter DL. The brain's default network. *Ann N Y Acad Sci*. 2008:1124(1):1–38.

Buzsáki G. Hippocampal sharp wave-ripple: a cognitive biomarker for episodic memory and planning. *Hippocampus*. 2015:25(10): 1073–1188.

Chrastil ER. Heterogeneity in human retrosplenial cortex: a review of function and connectivity. *Behav Neurosci*. 2018:132(5):317–338.

Clement EA, Richard A, Thwaites M, Ailon J, Peters S, Dickson CT. Cyclic and sleep-like spontaneous alternations of brain state under urethane anaesthesia. *PLoS One*. 2008:3(4):e2004.

Cowan E, Liu A, Henin S, Kothare S, Devinsky O, Davachi L. Sleep spindles promote the restructuring of memory representations in ventromedial prefrontal cortex through enhanced hippocampal-cortical functional connectivity. *J Neurosci*. 2020:40(9):1909–1919.

Cox R, Schapiro AC, Manoach DS, Stickgold R. Individual differences in frequency and topography of slow and fast sleep spindles. *Front Hum Neurosci*. 2017:11:433.

Donahue M, Kaszas A, Turi G, Rózsa B, Slézia A, Vanzetta I, Katona G, Bernard C, Malliaras G, Williamson A. Multimodal characterization of neural networks using highly transparent electrode arrays. *eNeuro*. 2018:5(6):ENEURO.0187–18.2018. https://doi.org/10.1523/ENEURO.0187-18.2018.

Foster DJ, Wilson MA. Reverse replay of behavioural sequences in hippocampal place cells during the awake state. *Nature*. 2006:440(7084):680–683.

Geva-Sagiv M, Nir Y. Local sleep oscillations: implications for memory consolidation. *Front Neurosci*. 2019:13:813.

Girardeau G, Benchenane K, Wiener SI, Buzsáki G, Zugaro MB. Selective suppression of hippocampal ripples impairs spatial memory. *Nat Neurosci*. 2009:12(10):1222–1223.

Girardeau G, Cei A, Zugaro M. Learning-induced plasticity regulates hippocampal sharp wave-ripple drive. *J Neurosci*. 2014:34(15): 5176–5183.

Gorgoni M, Lauri G, Truglia I, Cordone S, Sarasso S, Scarpelli S, Mangiaruga A, D'Atri A, Tempesta D, Ferrara M, et al. Parietal fast sleep spindle density decrease in Alzheimer's disease and amnesic mild cognitive impairment. *Neural Plast*. 2016:2016: 8376108–8376110.

Greenberg A, Abadchi JK, Dickson CT, Mohajerani MH. New waves: rhythmic electrical field stimulation systematically alters spontaneous slow dynamics across mouse neocortex. *NeuroImage*. 2018:174:328–339.

Helfrich RF, Lendner JD, Mander BA, Guillen H, Paff M, Mnatsakanyan L, Vadera S, Walker MP, Lin JJ, Knight RT. Bidirectional prefrontal-hippocampal dynamics organize information transfer during sleep in humans. *Nat Commun*. 2019:10(1):3572.

Higgins C, Liu Y, Vidaurre D, Kurth-Nelson Z, Dolan R, Behrens T, Woolrich M. Replay bursts in humans coincide with activation of the default mode and parietal alpha networks. *Neuron*. 2021:109(5):882–893.e7.

Ji D, Wilson MA. Coordinated memory replay in the visual cortex and hippocampus during sleep. *Nat Neurosci*. 2007:10(1):100–107.

Johnson LA, Euston DR, Tatsuno M, McNaughton BL. Stored-trace reactivation in rat prefrontal cortex is correlated with down-to-up state fluctuation density. *J Neurosci*. 2010:30(7):2650–2661.

Kaplan R, Adhikari MH, Hindriks R, Mantini D, Murayama Y, Logothetis NK, Deco G. Hippocampal sharp-wave ripples influence selective activation of the default mode network. *Curr Biol*. 2016:26(5):686–691.

Karimi, Abadchi J, Nazari-Ahangarkolaee M, Gattas S, Bermudez–Contreras E, Luczak A, McNaughton BL, Mohajerani MH. Spatiotemporal patterns of neocortical activity around hippocampal sharp-wave ripples (Biorxiv). 2020.

Karimi Abadchi J, Nazari-Ahangarkolaee M, Gattas S, Bermudez–Contreras E, Luczak A, McNaughton BL, Mohajerani MH. Spatiotemporal patterns of neocortical activity around hippocampal sharp-wave ripples. *Elife*. 2020:9:e51972.

Khodagholy D, Doublet T, Quilichini P, Gurfinkel M, Leleux P, Ghestem A, Ismailova E, Hervé T, Sanaur S, Bernard C, et al. In vivo recordings of brain activity using organic transistors. *Nat Commun*. 2013:4(1):1575.

Khodagholy D, Gelinas JN, Thesen T, Doyle W, Devinsky O, Malliaras GG, Buzsáki G. NeuroGrid: recording action potentials from the surface of the brain. *Nat Neurosci*. 2015:18(2):310–315.

Khodagholy D, Gelinas JN, Zhao Z, Yeh M, Long M, Greenlee JD, Doyle W, Devinsky O, Buzsáki G. Organic electronics for high-resolution electrocorticography of the human brain. *Sci Adv*. 2016:2(11):e1601027.

Kim D, Hwang E, Lee M, Sung H, Choi JH. Characterization of topographically specific sleep spindles in mice. *Sleep*. 2015:38(1):85–96.

Kyweriga M, Sun J, Wang S, Kline R, Mohajerani MH. A large lateral craniotomy procedure for mesoscale wide-field optical imaging of brain activity. *J Vis Exp*. 2017:(123):52642. https://doi.org/10.3791/52642.

Latchoumane C-FV, Ngo H-VV, Born J, Shin H-S. Thalamic spindles promote memory formation during sleep through triple phase-locking of cortical, thalamic, and hippocampal rhythms. *Neuron*. 2017:95(2):424–435.e6.

Lopes-dos-Santos V, Ribeiro S, Tort AB. Detecting cell assemblies in large neuronal populations. *J Neurosci Methods*. 2013:220(2): 149–166.

Lopes-Dos-Santos V, van de Ven GM, Morley A, Trouche S, Campo-Urriza N, Dupret D. Parsing hippocampal theta oscillations by nested spectral components during spatial exploration and memory-guided behavior. *Neuron*. 2018:100(4):940–952.e7.

Lu H, Zou Q, Gu H, Raichle ME, Stein EA, Yang Y. Rat brains also have a default mode network. *PNAS*. 2012:109(10):3979–3984.

Maingret N, Girardeau G, Todorova R, Goutierre M, Zugaro M. Hippocampo-cortical coupling mediates memory consolidation during sleep. *Nat Neurosci*. 2016:19(7):959–964.

Marr D, Willshaw D, McNaughton B. Simple memory: a theory for Archicortex In: Vaina L, editor. *From the retina to the neocortex: selected papers of David Marr*. Boston, MA: Birkhäuser; 1991, pp. 59–128. https://doi.org/10.1007/978-1-4684-6775-8_5.

McClelland JL, McNaughton BL, O'Reilly RC. Why there are complementary learning systems in the hippocampus and neocortex: insights from the successes and failures of connectionist models of learning and memory. *Psychol Rev*. 1995:102(3):419–457.

Mohajerani MH, Chan AW, Mohsenvand M, LeDue J, Liu R, McVea DA, Boyd JD, Wang YT, Reimers M, Murphy TH. Spontaneous cortical activity alternates between motifs defined by regional axonal projections. *Nat Neurosci*. 2013:16(10):1426–1435.

Nádasdy Z, Hirase H, Czurkó A, Csicsvari J, Buzsáki G. Replay and time compression of recurring spike sequences in the hippocampus. *J Neurosci*. 1999:19(21):9497–9507.

Nazari M, Abadchi JK, Naghizadeh M, Bermudez-Contreras EJ, McNaughton BL, Tatsuno M, Mohajerani MH. Regional variation in cholinergic terminal activity determines the non-uniform occurrence of cortical slow waves during REM sleep in mice. *Cell Rep*. 2023:42:112450. https://doi.org/10.1016/j.celrep.2023.112450.

Ngo H-V, Fell J, Staresina B. Sleep spindles mediate hippocampal-neocortical coupling during long-duration ripples. *elife*. 2020:9:e57011.

Niethard N, Ngo H-VV, Ehrlich I, Born J. Cortical circuit activity underlying sleep slow oscillations and spindles. *PNAS*. 2018:115(39):E9220–E9229.

Nitzan N, McKenzie S, Beed P, English DF, Oldani S, Tukker JJ, Buzsáki G, Schmitz D. Propagation of hippocampal ripples to the neocortex by way of a subiculum-retrosplenial pathway. *Nat Commun*. 2020:11(1):1947.

Nitzan N, Swanson R, Schmitz D, Buzsáki G. Brain-wide interactions during hippocampal sharp wave ripples. *Proc Natl Acad Sci*. 2022:119(20):e2200931119.

Ólafsdóttir HF, Carpenter F, Barry C. Coordinated grid and place cell replay during rest. *Nat Neurosci*. 2016:19(6):792–794.

Oliva A, Fernández-Ruiz A, Buzsáki G, Berényi A. Role of hippocampal CA2 region in triggering sharp-wave ripples. *Neuron*. 2016:91(6):1342–1355.

Opalka AN, Huang W, Liu J, Liang H, Wang DV. Hippocampal ripple coordinates retrosplenial inhibitory neurons during slow-wave sleep. *Cell Rep*. 2020:30(2):432–441.e3.

Pedrosa R, Nazari M, Mohajerani MH, Knöpfel T, Stella F, Battaglia FP. Hippocampal gamma and sharp wave/ripples mediate bidirectional interactions with cortical networks during sleep. *Proc Natl Acad Sci*. 2022a:119(44):e2204959119.

Pedrosa R, Song C, Knöpfel T, Battaglia F. Combining cortical voltage imaging and hippocampal electrophysiology for investigating global, multi-timescale activity interactions in the brain. *Int J Mol Sci*. 2022b:23(12):6814.

Peigneux P, Laureys S, Fuchs S, Collette F, Perrin F, Reggers J, Phillips C, Degueldre C, Del Fiore G, Aerts J, et al. Are spatial memories strengthened in the human hippocampus during slow wave sleep? *Neuron*. 2004:44(3):535–545.

Peyrache A, Khamassi M, Benchenane K, Wiener SI, Battaglia FP. Replay of rule-learning related neural patterns in the prefrontal cortex during sleep. *Nat Neurosci*. 2009:12(7):919–926.

Peyrache A, Battaglia FP, Destexhe A. Inhibition recruitment in prefrontal cortex during sleep spindles and gating of hippocampal inputs. *Proc Natl Acad Sci*. 2011:108(41):17207–17212.

Pinault D. The thalamic reticular nucleus: structure, function and concept. *Brain Res Rev*. 2004:46(1):1–31.

Rolls ET. Hippocampo-cortical and cortico-cortical backprojections. *Hippocampus*. 2000:10(4):380–388.

Rothschild G, Eban E, Frank LM. A cortical–hippocampal–cortical loop of information processing during memory consolidation. *Nat Neurosci*. 2017:20(2):251–259.

Sessolo M, Khodagholy D, Rivnay J, Maddalena F, Gleyzes M, Steidl E, Buisson B, Malliaras G. Easy-to-fabricate conducting polymer microelectrode arrays. *Adv Mater*. 2013:25(15):2135–2139.

Siapas AG, Wilson MA. Coordinated interactions between hippocampal ripples and cortical spindles during slow-wave sleep. *Neuron*. 1998:21(5):1123–1128.

Sirota A, Csicsvari J, Buhl D, Buzsaki G. Communication between neocortex and hippocampus during sleep in rodents. *Proc Natl Acad Sci USA*. 2003:100(4):2065–2069.

Skelin I, Zhang H, Zheng J, Ma S, Mander BA, Kim McManus O, Vadera S, Knight RT, McNaughton BL, Lin JJ. Coupling between slow waves and sharp-wave ripples engages distributed neural activity during sleep in humans. *Proc Natl Acad Sci*. 2021:118(21):e2012075118.

Song C, Piscopo DM, Niell CM, Knöpfel T. Cortical signatures of wakeful somatosensory processing. *Sci Rep*. 2018:8(1):11977.

Staresina BP, Bergmann TO, Bonnefond M, van der Meij R, Jensen O, Deuker L, Elger CE, Axmacher N, Fell J. Hierarchical nesting of slow oscillations, spindles and ripples in the human hippocampus during sleep. *Nat Neurosci*. 2015:18(11):1679–1686.

Staresina BP, Niediek J, Borger V, Surges R, Mormann F. How coupled slow oscillations, spindles and ripples coordinate neuronal processing and communication during human sleep. *Nat Neurosci*. 2023:26(8):1429–1437.

Stickgold R, Walker MP. Memory consolidation and reconsolidation: what is the role of sleep? *Trends Neurosci*. 2005:28(8):408–415.

Tambini A, Davachi L. Awake reactivation of prior experiences consolidates memories and biases cognition. *Trends Cogn Sci*. 2019:23(10):876–890.

Tambini A, Ketz N, Davachi L. Enhanced brain correlations during rest are related to memory for recent experiences. *Neuron*. 2010:65(2):280–290.

Timofeev I, Steriade M. Low-frequency rhythms in the thalamus of intact-cortex and decorticated cats. *J Neurophysiol*. 1996:76(6):4152–4168.

Tong APS, Vaz AP, Wittig JH, Inati SK, Zaghloul KA. Ripples reflect a spectrum of synchronous spiking activity in human anterior temporal lobe. *elife*. 2021:10:e68401.

Vann SD, Aggleton JP, Maguire EA. What does the retrosplenial cortex do? *Nat Rev Neurosci*. 2009:10(11):792–802.

Wang DV, Ikemoto S. Coordinated interaction between hippocampal sharp-wave ripples and anterior cingulate unit activity. *J Neurosci*. 2016:36(41):10663–10672.

Wang S-H, Morris RGM. Hippocampal-neocortical interactions in memory formation, consolidation, and reconsolidation. *Annu Rev Psychol*. 2010:61(1):49–79.

Wilson MA, McNaughton BL. Dynamics of the hippocampal ensemble code for space. *Science*. 1993:261(5124):1055–1058.

Xu W, De Carvalho F, Clarke AK, Jackson A. Communication from the cerebellum to the neocortex during sleep spindles. *Prog Neurobiol*. 2021:199:101940. https://doi.org/10.1016/j.pneurobio.2020.101940.